The sintering mechanism of fully dense and highly coercive Nd-Fe-B magnets from the recycled HDDR powders reprocessed by spark plasma sintering

Ikram, Awais; Mehmood, Muhammad Farhan; Podlogar, Mateja; Eldosouky, Anas; Sheridan, Richard; Awais, Muhammad; Walton, Allan; Krzmanc, Marteja; Tomse, Tomaz; Kobe, Spomenka; Sturm, Saso; Rozman, Kristina Zuzek

DOI:
10.1016/j.jallcom.2018.09.322

Document Version
Publisher's PDF, also known as Version of record

Citation for published version (Harvard):
Ikram, A, Mehmood, MF, Podlogar, M, Eldosouky, A, Sheridan, R, Awais, M, Walton, A, Krzmanc, M, Tomse, T, Kobe, S, Sturm, S & Rozman, KZ 2019, 'The sintering mechanism of fully dense and highly coercive Nd-Fe-B magnets from the recycled HDDR powders reprocessed by spark plasma sintering', *Journal of Alloys and Compounds*, vol. 774, pp. 1195-1206. https://doi.org/10.1016/j.jallcom.2018.09.322

Journal of Alloys and Compounds 774 (2019) 1195–1206

Contents lists available at ScienceDirect

Journal of Alloys and Compounds

journal homepage: http://www.elsevier.com/locate/jalcom

The sintering mechanism of fully dense and highly coercive Nd-Fe-B magnets from the recycled HDDR powders reprocessed by spark plasma sintering

Awais Ikram [a, b, *], M. Farhan Mehmood [a, b], Mateja Podlogar [a], Anas Eldosouky [b, d], Richard Stuart Sheridan [c], Muhammad Awais [c], Allan Walton [c], Marjeta Maček Kržmanc [e], Tomaz Tomse [a, b], Spomenka Kobe [a, b], Saso Sturm [a, b], Kristina Žužek Rožman [a, b]

[a] Department for Nanostructured Materials, Jožef Stefan Institute, Jamova cesta 39, SI-1000, Ljubljana, Slovenia
[b] Jožef Stefan International Postgraduate School, Jamova cesta 39, SI-1000, Ljubljana, Slovenia
[c] School of Metallurgy and Materials, University of Birmingham, Edgbaston, Birmingham, B15 2TT, United Kingdom
[d] Magneti Ljubljana, d.d., Stegne 37, SI-1000, Ljubljana, Slovenia
[e] Advanced Materials Department, Jožef Stefan Institute, Jamova cesta 39, Ljubljana, 1000, Slovenia

ARTICLE INFO

Article history:
Received 19 June 2018
Received in revised form
24 September 2018
Accepted 25 September 2018
Available online 26 September 2018

Keywords:
Rare earth
Permanent magnets
$Nd_2Fe_{14}B$
Recycling
Spark plasma sintering
Reprocessing
Coercivity
HDDR
HD
Nanocrystalline

ABSTRACT

The goal of this study was to justify the reprocessing of recycled HDDR Nd-Fe-B powders with spark plasma sintering (SPS) and to investigate the dependence of the final magnetic properties on SPS and thermal treatment. The initial recycled HDDR powder of the composition $Nd_{13.4}Dy_{0.6}Fe_{78.6}B_{6.1}Nb_{0.4}Al_{0.7}$ with 4760 ppm O_2 content, coercivity (H_{Ci}) = 830 kA/m, and large particle size distribution <50–600 μm, was treated using the SPS parameters as follows: T = 650–850 °C for 1–5 min and 50 MPa pressure. The post SPS thermal treatment was performed at 750 °C for 15 min in vacuum. The optimal SPS conditions at 750 °C for 1 min, yielded fully dense magnets with the coercivity H_{Ci} = 1060 kA/m, which was boosted to 1160 kA/m after the post-SPS thermal treatment. The grain growth was obvious in samples SPS-ed above 800 °C and subsequently, the H_{Ci} was reduced. The SPS reprocessing beyond 850 °C was found to be detrimental to the overall magnetic properties due to the formation of bimodal grain size distribution origination from the abnormal grain growth (700–2600 nm). The redistribution of Nd-rich grain boundary phase between the $Nd_2Fe_{14}B$ matrix grains in thermally treated magnets and the relaxation of the internal stresses induced via SPS are the possible reasons for the H_{Ci} surpassing the H_{Ci} of the starting recycled HDDR powder. It was shown that the SPS consolidation technique is suitable for producing fully dense nanograined bulk Nd-Fe-B magnets, with coercivities even exceeding the initial HDDR-powder and is one of the most suitable routes for revitalizing the Nd-Fe-B scrap magnets.

1. Introduction

Since the discovery of the rare-earth-based Nd-Fe-B type permanent magnets in 1984 [1,2], they became essential in energy, telecommunication, microelectronics and aerospace applications, as well in medical equipment, computers, sensors, electric motors and fusion devices [3–5]. However, in 2011, the rare earth elements (REE) importers met a supply chain crisis and as a result, the prices soared [6]. Since the REE are a backbone for the green technologies, the EU now considers them as the most critical raw materials in terms of supply risk [6]. In comparison with the light rare earth elements (LREE), the heavy rare earth elements (HREE) like Dy, Tb, Ho etc. are more scarce and hence, more expensive. Dy is consistently used as a dopant to increase coercivity in high-performance permanent magnets, suitable for applications above 100 °C [4,6]. This, however, decreases the remanence (B_r) and the BH_{max}, due to the antiferromagnetic coupling of Dy with Fe atoms. Increasing the coercivity (H_{Ci}) of Nd-Fe-B magnets without the HREE addition can be done via grain boundary modification treatments, which increases the grain boundary phase thickness in a way that neighboring grains become magnetically decoupled [4]. The other option

* Corresponding author. Department for Nanostructured Materials, Jožef Stefan Institute, Jamova cesta 39, SI-1000, Ljubljana, Slovenia.
E-mail address: awais.ikram@ijs.si (A. Ikram).

https://doi.org/10.1016/j.jallcom.2018.09.322

is to develop near single domain nanostructured $Nd_2Fe_{14}B$ grains (≤400 nm). This can be achieved via melt spinning or by utilizing the Hydrogenation-Disproportionation-Desorption-Recombination (HDDR) process [5]. The grain size refinement is considered a very viable option as it enhances the H_{Ci} [4] without HREE addition. However, such nanograined powder cannot be manufactured via the conventional sintering route, as the $Nd_2Fe_{14}B$ grains will grow exponentially with temperature exceeding 1000 °C and the H_{Ci} will be lost [4,5], therefore alternative processing routes have to be proposed.

In view of the REE crisis and knowing that the industrial processing wastes in permanent magnet production accounts to ≥25% for REE [7,8] it became feasible to recycle and reprocess them. The end-of-life (EOL) permanent magnets can be recycled using the hydrogen decrepitation process [8] to form non-magnetic powders, which can further be reprocessed and reused as suggested by Li Xiantao et al. [7]. Several researchers [7–19] have reported with varying degree of success on recycling the scrap Nd-Fe-B and reprocessing by conventional sintering of hydrogen decrepitated (HD) and jet-milled recycled powder [8,9]. However, to date, no trials have been made on the sintered magnets from recycled HDDR powders and only low H_{Ci} bonded magnets have been reported [7]. The HDDR reprocessing has been utilized in recycling by Walton et al. [9] and Sheridan et al. [13] to make nanocrystalline powders, but for bonded magnet applications only. However, the reports from McGuiness [20] and Mueller [21] on Zr-doped hot pressed HDDR powders indicate that fully dense magnets can be processed without a significant loss in the H_{Ci} compared to the starting powder. It is evident that the rapid compaction techniques e.g. shock compaction can be used in the alternate strategy to develop nanocrystalline bulk sintered Nd-Fe-B magnets without degrading their H_{Ci} [5]. The Spark Plasma Sintering (SPS) compaction method would represent a suitable alternative to produce dense magnets. The SPS-ed fresh and commercial grade HDDR Nd-Fe-B powder was already processed by Suresh et al. [22] and Takagi et al. [23], which have indicated the possibility to fully densify the HDDR powders within a few minutes at 600–750 °C. These corresponding SPS temperatures are 30–40% lower than the ones used in conventional vacuum sintering (>1050 °C). However, after SPS-ing the H_{Ci} was lost and only regained subsequently by post-sinter annealing treatments, attributed to the redistribution of the Nd-rich grain boundary phase and the intergrain stress relaxation [22–26]. The reason for this overall low H_{Ci} in compacted samples having near single domain structure has been attributed to inadequate grain isolation, by only a thin paramagnetic Nd-rich grain boundary phase, identified previously by Gopalan et al. [24] and Li et al. [25]. To achieve adequate localized grain decoupling, enough paramagnetic Nd-rich phase must be uniformly distributed between the matrix grains and for this reason, the excess Nd is added to the composition to compensate for the Nd-loss due to oxidation during the recycling process [4,10,15]. With the focus of increasing the BH_{max}, tackling the remnant magnetization is also one of the major factors, however, compacted HDDR powders express usually low remanence (B_r) which is reasoned to a poor degree of easy axis alignment (texture) after compaction [24]. The mechanism for microstructure development in the HDDR powder consolidated with the SPS is still to be determined, and only then the SPS parameters and resultant microstructure can be controlled for maximizing the H_{Ci} of near single domain grained HDDR powder.

Our study proposes the reprocessing of HDDR powders from EOL magnetic scrap using the SPS process for the first time, to contribute to the already existing state-of-the-art of the nanocrystalline HDDR Nd-Fe-B powders. The EOL scrap magnet HDDR powder in comparison to the "fresh/commercial" HDDR powder has a higher overall oxygen content, therefore obtaining high H_{Ci} presents a challenge with such Nd-Fe-B system. As K. Takagi et al. [23] reported that the particle size distribution is crucial in determining the H_{Ci} of SPS-ed HDDR powder, as different HDDR particle fractions were associated with the different degree of surface oxidation, leading to lower H_{Ci} for smaller particles. However, to date, the H_{Ci} decrease due to oxidation has not been yet fully understood in terms of the microstructure [23,27,28]. Unlike commercial or fresh SPS-ed HDDR powder in which the H_{Ci} drops after SPS and the properties have to be recovered with proper annealing treatment [23], we have demonstrated that a direct SPS reprocessing of the recycled HDDR powders with near stoichiometric composition, does result in even higher H_{Ci} than the starting HDDR powder. The combination of rapid high-temperature SPS and thermal treatment above the eutectic temperature allowed us to preserve the grains from growing, achieving full densification and redistributing the Nd-rich grain boundary phase, diminishing the intergranular stresses and increasing the H_{Ci}. This research work approves the application of SPS for developing nanostructured sintered magnets, even from the recycled HDDR Nd-Fe-B powders.

2. Experimental

The original end-of-life (EOL) sintered Nd-Fe-B magnets had $H_{Ci} = 1170$ kA/m and $B_r = 1.19$ T. These EOL magnets were HD treated and pulverized to reduce particle size. Further, these particles were HDDR reprocessed; complete details of this process has been previously reported by Sheridan et al. [13,29] for producing the anisotropic recycled powder. The EOL scrap magnet has an overall oxygen content of 2660 ppm (0.266 wt %). After the HDDR process, the oxygen content increased to 4760 ppm (0.476 wt %). The intrinsic magnetic properties of recycled HDDR powder were measured as a bonded magnet with the Lakeshore VSM (not adjusting for self-demagnetization). The measured J_S value accounts to 1.4 T. The EOL sintered magnets having a nominal composition of $Nd_{13.4}Dy_{0.6}Fe_{78.6}B_{6.1}Nb_{0.4}Al_{0.7}$ measured with Inductively Coupled Plasma Mass Spectroscopy (ICP-MS) were HD treated and then the dynamic hydrogenation-disproportionation-desorption-recombination (d-HDDR) process was utilized to develop recycled powder with nanostructured anisotropic grains. Detailed description of HDDR processing is provided by Sheridan et al. [13]. The theoretical density was calculated by measuring the weight fraction of the individual elements with the respective density of each element in the HDDR powder composition and it was approximated to 7.57 ± 0.01 g/cm^3. This recycled HDDR powder had a wide particle size distribution as measured from HR-SEM. The phase analysis for the recycled HDDR powder was performed using the XRD (PANalytical Empyrean Diffractometer).

The Curie temperature (T_C), endothermic eutectic melting and exothermic crystallization processes were determined by Thermogravimetric Differential Scanning Calorimetry (TG-DSC) in the temperature range of 30–900 °C with the heating and cooling rates of 20 °C/min, under argon environment (99.99% purity, flow rate 50 ml/min) using Jupiter 449 Simultaneous Thermal Analysis (STA) instrument with TG-DSC-cp sample holder and Pt-crucibles with Al_2O_3 liners. The temperature and sensitivity calibration of the instrument was performed with In, Bi, Zn, Al and Au standards. Before the DSC analysis, the samples were exposed to air atmosphere only for a few minutes during weighing before repeated vacuuming (5×10^{-4} mbar) and purging with Argon. The oxygen content of the HDDR powder and particle fractions was measured by Eltra ON 900, oxygen and nitrogen analyzer. In order to estimate the average particle size, the sieving of HDDR powder was performed from 1 mm sieve down to <50 μm sieve size in a glove box to prevent any oxidation of the recycled powder before the XRD, the microstructural characterization and the SPS reprocessing.

For the preparation of the SPS sintered magnets out of the recycled HDDR powder, the cylindrical graphite dies of 16 mm internal diameter were used and 5 g of the recycled HDDR powder was added in between the graphite foils and spacers. Punches were placed in to squeeze the powder compactly. Further pre-pressing or magnetic pre-alignment of the HDDR powders in the graphite molds was not performed before sintering for making isotropic magnets. These prepared molds were then placed in Syntex 3000 (DR. SINTER) SPS furnace with controlled pressure unit and a thermocouple. All the SPS experiments were performed under a vacuum of 2×10^{-2} mbar and a constant uniaxial pressure of 50 MPa was maintained. The sintering temperature was varied from 650 to 850 °C, with a heating ramp of 50 °C/minute. The holding time at the sintering temperature was kept from 1 to 5 min (s). The SPS temperature was controlled with a calibrated thermocouple. All the SPS-ed samples were grinded using 500 grit size SiC papers to peel off the graphite spacers. Fine grinding up to 4000 grit was done further and the samples were polished on rotary disks using 1/4 μm diamond paste on the velvet cloth. Samples were then analyzed for the magnetic properties on a permeameter (Magnet-Physik Dr. Steingroever) by taking successive magnetization and demagnetization measurements. The density measurements were taken on density-meter (DENSITEC) utilizing the Archimedean principle and immersed in silicone oil.

Post-sinter thermal treatments (PST) were performed under a vacuum of $>10^{-5}$ mbar at a heating rate of 50 °C/minute in a horizontal tube furnace. The isothermal annealing temperature was kept at 750 °C and the samples were held for 15 min at this temperature. The density and magnetic measurements were repeated after the annealing step. For the microstructural investigations SPS-ed and post thermally treated samples etched with 3M Cyphos. The microstructural investigation was performed on the recycled etched and non-etched HDDR powder, the SPS-ed and the PST specimens using Field Emission Scanning Electron Microscope (JEOL 7600F and FEI Helios NanoLab DualBeam 650 FIB with Oxford Aztec 50 mm^2). Electron energy dispersive X-ray spectroscopy (EDS) was performed at 20 keV.

3. Results and discussion

3.1. Chemical, thermal, magnetic and crystal structure characterization of the recycled HDDR powder

In order to investigate the thermal behaviour of the starting HDDR powder to determine the SPS regime, thermal analysis was performed. Fig. 1 (a) illustrates the typical TG and DSC curves obtained for recycled HDDR powder during heating at a heating rate of 20 °C/min to 900 °C peak temperature. The increase of mass due to oxidation during thermal analysis experiment was not significant (0.23%) and as it is very small and continuous (500–900 °C), its contribution to thermal effects could be neglected. DSC heating curve in Fig. 1 (a) is characterized by several endothermic effects. The low-temperature DSC peak, which was noticed at 307 °C, belongs to the Curie temperature (T_C) of the Nd-Fe-B. The onset of T_C begins close to 260 °C. The enthalpy associated with this phase transition was 4.9 J/g, which is significant for this transition after several repeated experiments. Further on, the most intense DSC peak is observed at 743 °C with its transformation on-set at 665 °C. This DSC peak is very close to the already reported ternary eutectic temperature T_{ELM} (690 °C), where $Nd_2Fe_{14}B$ matrix phase is present with liquefied α-Nd [39], however slightly lower on-set temperature (665 °C) observed for HDDR powder in this study could be related to the presence of other elements such as Dy, Nb and Al in very low quantity, which might lower this eutectic temperature. Similarly, Vial et al. [42] also determined the eutectic temperature lower than 690 °C (646 °C) for the composition $Nd_{12.4}Pr_{1.4}B_{5.8}Al_{0.3}Cu_{0.1}Fe_{79.9}$, which was very similar to the material used in this work. In the DSC curve of this alloy with a minor content of Al, Cu and Co an additional endothermic peak was also noticed at 527 °C by the authors [42]. This peak could originate from Co and Cu containing compounds with a low melting temperature. Although Co and Cu are not constituents of the HDDR powder in the present study, a weak endothermic peak was observed in the lower temperature range at 477 °C. The measured enthalpy (0.6 J/g) associated with this low-temperature melting was considerably smaller than the characteristic (6.7 J/g) determined for the melting at higher temperature eutectic transformation between 665 °C and 770 °C. The formation of a low-temperature endothermic reaction in both systems containing Al implies that this melting is perhaps related to Al and its interactions in the system with Dy and Nd at the grain boundary interface. The enhanced melting effect of the grain boundary phase due to the presence of Al and Ni was already reported by N. Oono et al. [32].

In the cooling DSC curves of the HDDR powder, the exothermic peak belonging to the paramagnetic to ferromagnetic phase transition is well defined (Fig. 1b). The onset begins close to 310 °C and the peak corresponds to $T_c = 293$ °C for HDDR powder, so the results match during heating and cooling runs. The cooling DSC curve of HDDR powder was additionally characterized by weak and broad exothermic peak extending from 760 °C to 700 °C, which could be ascribed to the crystallization of the Nd-rich grain boundary phase. Since this process was associated with a rather small change of enthalpy (0.7 J/g) we can assume that during cooling with the rate of 20 °C/min the majority of grain boundary phase may possibly end up amorphous instead of well-defined crystalline grain boundaries due to the absence of well-defined peak(s). DSC measurements of the recycled HDDR powder samples were performed several times and very reproducible results were obtained. The initial Dy and Al additions to bulk magnets are reasoned to reduce this grain boundary phase melting temperature [32,33,39]. Therefore, the SPS reprocessing temperatures were kept in the 650–850 °C range to correlate the effect of the temperature to the microstructural evolution and its result on the magnetic properties, which will be discussed later. These measured values of T_C and T_{ELM} are synonymous with the work done by Hono et al. [39] on Nd-Fe-B.

The XRD analysis of the HDDR recycled powder is shown in Fig. 2. The reflections correspond to the tetragonal $Nd_2Fe_{14}B$ hard magnetic phase with JCPDA reference numbers 00-036-1296 and 04-006-2691 as the major phase. The lattice parameters of matrix phase are: a = 8.79 (Å), b = 8.79 (Å) and c = 12.2 (Å), with *P*42/*mnm* space group and space group number of 136. As the scrap magnet contained 0.6 at. % Dy, the $DyNdFe_{14}B$ phase (JCPDA # 01-089-3548) with multiple overlapping peaks can be adjusted with the similar lattice parameters: a = 8.79 (Å), b = 8.79 (Å), c = 12.1 (Å) and *P*42/*mnm* space group. The Nd-oxide phases were also detected by XRD, attributing to the pickup of oxygen before and/or during the HDDR reprocessing. The cubic NdO_2 (JCPDA # 04-007-0500) and Nd_2O_3 (JCPDA # 00-040-1283) phases were detected. In addition, the $NdFe_4B_4$ (JCPDA # 01-081-3530) phase was also present in the recycled HDDR powder which was to be expected.

3.2. Characterization of the recycled HDDR powders

Fig. 3 shows the BSE SEM micrographs of polished recycled HDDR Nd-Fe-B powder prepared in epoxy resin. The particles have irregular shapes and a large particle size distribution, from 30 to 700 μm, with an average particle size of 220 μm. Fig. 3 (a) shows a typical microstructure of the HDDR powder whereby the grey matrix corresponds to $Nd_2Fe_{14}B$ (highlighted as 1) and the bright phases are Nd-rich intergranular phases, NdO_X (highlighted as 2)

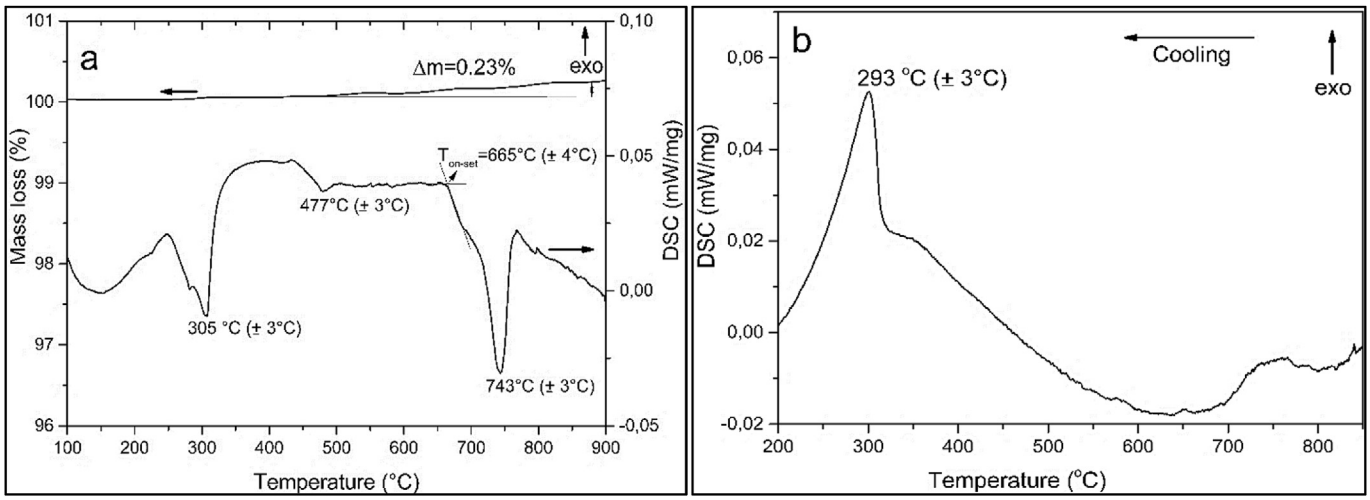

Fig. 1. TG and DSC curves of (a) the recycled HDDR Nd-Fe-B powder during (a) heating and (b) cooling.

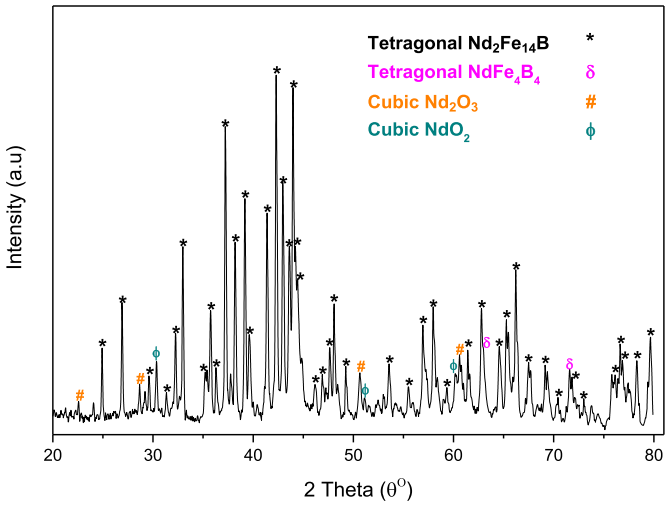

Fig. 2. Illustrates the XRD analysis of recycled HDDR powder.

and Nd_2O_3 (highlighted as 3) phases randomly scattered in the matrix. The EDS quantification of these phases is shown in Table 1. The darker contrast phases marked with "B" and "L" corresponding to $NdFe_4B_4$ type borides and $NbFe_2$ types Laves phases respectively. The Nb-rich phases are traced back from the EOL sintered scrap magnet forming $NbFe_2$ type Laves phases scattered in the Nd-Fe-B matrix which are nonetheless not significant in volume to be traced with the XRD analysis of the recycled HDDR powder. The Nb addition in sintered magnets also improves H_{Ci} such that the grains of a hard phase become more regular and the interfaces with grain boundaries get wider and smoother [30]. Nb reportedly forms $NbFe_2$ Laves phase during the recombination reaction, such that precipitation of α-Fe is suppressed, as α-Fe is known to substantially reduce the H_{Ci} [30,31]. The Laves phase reappears in the recycled HDDR powder as quantified in EDS results in Table 1 and therefore no free bcc iron (α-Fe) was detected with either EDS or XRD. The other dark grey phase corresponds to the conversion of the boride phase from Fe_2B phase to $NdFe_4B_4$ type phase after the HDDR reaction [52]. SEM-EDS cannot accurately quantify boron, but Nd:Fe ratio of 1:4 was detected from this phase as shown in Table 1.

Upon etching the matrix grains became more apparent and are shown in Fig. 3 (b), as the Nd-rich phases were selectively removed, except the Nd_2O_3 oxides (as the bright phase marked as 3 in the inset of Fig. 3b). Most of the bright phases along the grain boundaries have an approximate atomic ratio Nd:O of 1:2 (Table 1) which indicates the chemical composition to NdO_X (NdO_2) type Nd-rich phases. The protruding light greyish Nd-rich features with Nd:O elemental ratio of 2:3 (Table 1), pointing to the presence of Nd_2O_3 type oxide as identified with the XRD. These oxides are randomly scattered in the recycled HDDR powder along the particle boundaries as obvious after etching in Fig. 3 (b), appearing in different morphologies and composition as discussed. The traces of Al were also observed at the interfaces of the Nd-rich grain boundaries and the $Nd_2Fe_{14}B$ matrix grains. The Al signal was also detected within the $Nd_2Fe_{14}B$ grains, and measured EDS values correspond to an overall $\leq$1.2 at. % Al in the Nd-Fe-B matrix phase. The Al addition has been reported to decrease the melting point of rare earth rich (Nd, Dy) grain boundary phase [32]. K. Morimoto et al. (2012) [33] reported that the addition of up to 2.5 at. % of Al causes the thickening of the Nd-rich grain boundary phase. Al is known to uniformly distribute the Nd-enriched phase from the triple junctions along the grain boundaries. This pins the domain walls at the grain boundaries and improves the isolation of the adjacent $Nd_2Fe_{14}B$ grains, increasing the overall powder H_{Ci} [33–35]. Higher magnification image of the nanocrystalline matrix grains in the recycled HDDR powder after etching is shown in Fig. 3 (c) and (d), with an average grain size in the range from 240 to 420 nm and a monomodal grain size distribution. In addition, there are also larger "residual" (marked as "R") micron-sized grains (2–10 μm) observed within the initial recycled powder which can be attributed to the incomplete HDDR reaction [29,52].

3.3. Magnetic properties and characterization of SPS reprocessed HDDR powder

After the HDDR reprocessing, the coercivity of the recycled powder as measured with the VSM (without self-demagnetization adjustment) was 830 kA/m. The first objective of our study was to find a range of SPS processing temperature where the recycled HDDR powder could be densified completely. The magnetic properties and density measurements for SPS-ed magnets in range of 650–850 °C and holding time of 1 min as shown in Fig. 4 indicate a very good possibility of obtaining fully dense Nd-Fe-B permanent magnets from recycled HDDR powders with SPS. At 650 °C, the

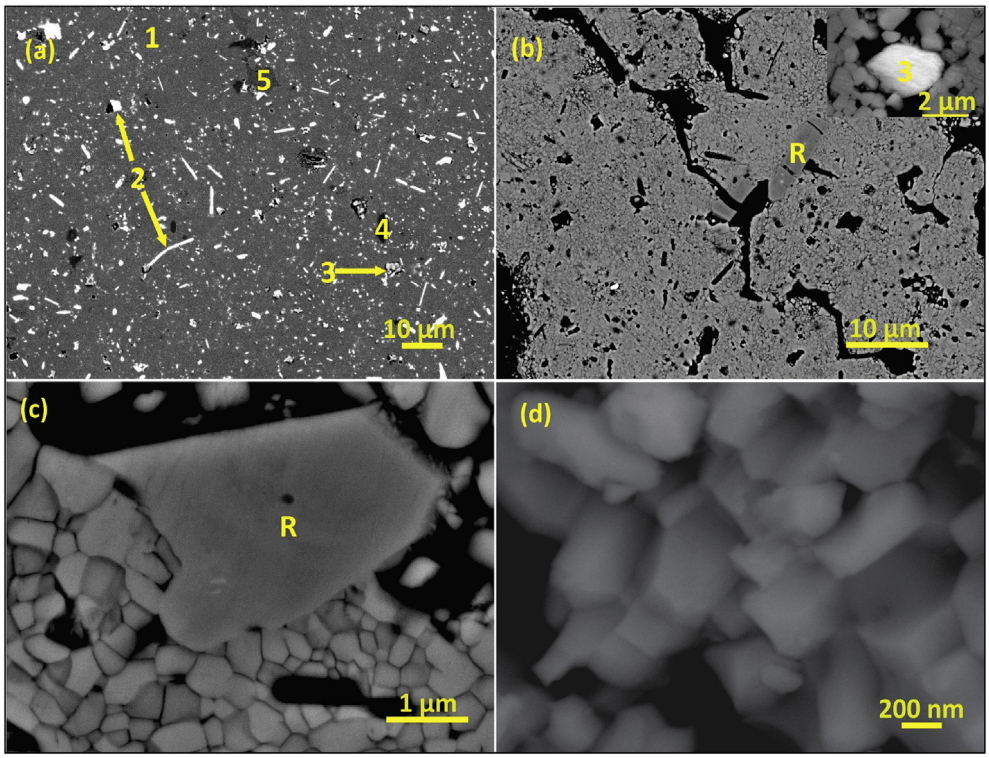

Fig. 3. HR-SEM BSE images of the initial recycled HDDR powder, (a) "1" $Nd_2Fe_{14}B$ matrix phase, "2" the bright Nd-rich grain boundary phase, "3" the Nd-oxide phase, "4" is Nb-Fe Laves phase and "5" are the $NdFe_4B_4$ type boride phase; (b) microstructure after etching; Nd-rich phases are etched away and nanocrystalline $Nd_2Fe_{14}B$ matrix grains are microscopically exposed; an inset shows Nd_2O_3 oxide phase marked with "3"; (c) higher magnification image of matrix phase consisting of mostly nanosized grains and approx. < 5 vol % fraction of large $Nd_2Fe_{14}B$ "R"- residual grains (not reacted during the HDDR process); (d) 50,000× magnification of a powder particle fracture surface showing 240–420 nm single crystal $Nd_2Fe_{14}B$ grains.

Table 1
EDS quantification of different phases in the recycled HDDR powder.

Phase Number	Phases	Nd (at. %)	Fe (at. %)	B (at. %)	O (at. %)	Nb (at. %)	Al (at. %)
1	$Nd_2Fe_{14}B$ Matrix	12.7	87.1	–	–	–	1.2
2	Nd-rich NdO_x/NdO_2	24.6	29.5	–	46.3	–	–
3	Nd_2O_3	35.2	12.2	–	47.3	–	–
4	$NbFe_2$ Laves	0.7	47.6	–	–	51.7	–
5	$NdFe_4B_4$ Boride	10.9	39.6	–	2.5	–	–

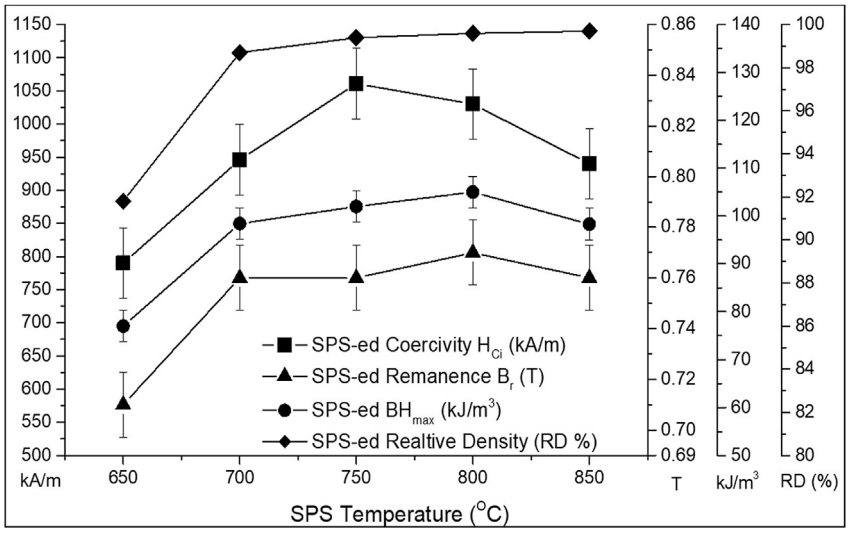

Fig. 4. The effect of SPS temperature on H_{Ci}, B_r, BH_{max} and density of the recycled HDDR Nd-Fe-B powders.

magnet density was only 91% of the theoretical value, however, the density was found to increase monotonically with the temperature and at T ≥ 700 °C where it starts to approach the theoretical value of 7.58 g/cm^3. Here we have to emphasize that it is possible to sinter the scrap Nd-Fe-B with the oxygen content greater than 4500 ppm even though it is known that Nd-oxide phases don't sinter well [44–47].

Fig. 4 shows that nearly full densification is possible due to grain consolidation and effective pore elimination with the SPS. The BH_{max} increases simultaneously with the B_r, which was found to increase with the reprocessing temperatures above 700 °C and reached the value of 0.77 T (105 kJ/m^3) in the sample SPS-ed at 800 °C. Since the powder particles are not aligned before the SPS, the measured remanence in this range (0.71–0.77 T) implies the isotropic nature of the Nd-Fe-B reprocessed magnets.

The recycled powder H_{Ci} = 830 kA/m increased further with SPS reprocessing temperature of 700 °C and reached a maximum value of 1061 ± 50 kA/m at the optimal SPS temperature of 750 °C as shown in Fig. 4. With the further increase in temperature, the H_{Ci} drops down slightly which can be associated with moderate grain growth. With increased oxygen content in the scrap magnet from 2660 ppm to 4760 ppm after HDDR reprocessing, one would expect slower sintering kinetics of the recycled HDDR powder, as some of the metallic Nd is scavenged by oxygen. So with a reduction of the overall Nd content i.e. the Nd-rich liquid phase, proper wetting of the grain boundary phase will be limited. The Nd oxides (Nd_2O_3 and NdO_2) remain in the solid state during sintering and appear along the triple pockets and the grain junctions. In the HDDR system, the matrix grains and grain boundary phases are nanosized, with a significantly higher surface area, so the regions for Nd scavenging and oxide precipitation are considerably higher. In order to increase the H_{Ci} of sintered [32] and the HDDR powder [33,34], the rare earth rich low-temperature eutectic alloys are blended into the compositions with leaner rare-earth content, which provides enough intergranular paramagnetic Nd-rich phase for the intergrain decoupling [24–26]. In the conventional vacuum sintering route, the oxygen content is always kept below the 4000 ppm limit for sinterability and usually, the excess amount of NdH_2 is added to counter the Nd-enrichment loss due to oxidation [10,15]. On the contrary, SPS enables concurrent localized coalescence/melting [48–50] of the Nd-rich grain boundary phase in the bulk powder, which promotes the wetting of the particles even with O_2 ~5000 ppm, therefore to an experimentally identified limit of O_2 < 8000 ppm, sintering of the HDDR reprocessed scrap is possible with the SPS.

The SPS experiments performed at 650 °C were below the eutectic temperature of the ternary phase transition (α-Nd + $Nd_2Fe_{14}B$ and $NdFe_4B_4$). In this case, we can only expect solid-state mass transport and Nd-rich phase will not experience redistribution, although rearrangement of the particles is made under 50 MPa uniaxial pressure. So the SPS coalescence together these particles with high heat transfer at particle necking regions by pulsed current resistance heating [48] and in effect the short range mass transport only fills out few pores which are apparent from the density of 6.9 g/cm^3 (91% densification). Fig. 5 (a) shows the unetched surface of sample SPS-ed at 650 °C, which can be correlated similarly to the recycled HDDR powder in terms of phase distribution and with several pores present, density is apparently lower (~90% densification). After etching in Fig. 5 (b), the average grain size range of SPS-ed samples at 650 °C is between 280 and 440 nm, with an exception of few larger sized grains approx. 1 μm. The SPS process changes from solid state sintering to liquid phase sintering when the SPS holding temperature is raised to 700 °C, which is above the ternary eutectic temperature. Under pressure, the recycled powder particles rearrange and the liquid phase diffuses towards the center of the powder particles into the grain boundaries at T ≥ 700 °C. A slightly higher temperature of 750 °C is optimal for the grain boundary diffusion during SPS, such that mass transport is efficient enough for near complete densification (99%) and pore annihilation as observed in the unetched specimen in Fig. 5 (c), but retaining a control with minimal grain growth as observed after etching in Fig. 5 (d). Near the Nd-rich pools the grain boundary phase acts as the spacers phase between the matrix grains, but the overall distribution of the grain boundary phase along the matrix grains and the particles are not uniform. The grain size distribution of recycled HDDR powder SPS-ed at 750 °C corresponds to 330 ± 120 nm. Apart from normally grown nanocrystalline grains of 330 ± 120 nm size at 750 °C, the slightly larger residual grains (≥5 μm) were also observed. When the SPS holding temperature was 850 °C, the coarsening of these "nanocrystalline" grains becomes apparent with an increase in average grain size to 750 ± 260 nm and some grains larger than several microns were also observed. At T_{SPS} > 850 °C, the grain growth rate is faster than the pore mobility which leads to the isolation of the pores within larger grains as neighboring grains coalesce together rapidly and begin to merge with a higher degree of faceting [51]. This results in the abnormal grain growth labelled with "A" in Fig. 5 (d and f), that causes the bimodal grain size distribution. This abnormal grain growth in samples SPS-ed at T > 800 °C is also one of the reasons for the H_{Ci} reduction.

The redistribution of the Nd-rich phase between the matrix grains is considered to improve the localized decoupling effect which increases the H_{Ci} [24,33–35]. Immediately after the removal of heat, the reprecipitation [51] of 2:14:1 matrix grains from solidifying Nd-rich phase causes pore eradication as the diffusion in the liquid phase augments the surfaces of the nanocrystalline grains and the grain boundary interfaces such that full densification is possible. This quick non-equilibrium sintering prevents any excessive mass transport of the liquid phase, and as the current stops, the cooling begins immediately which prevents grain coarsening [38]]. Due to the lack of Nd-rich phase at the grain boundaries in the commercial grade, HDDR powders after SPS-ing is accounted for a drastic H_{Ci} drop since the Nd-rich phase is absent between matrix grains and a significant localized exchange coupling effect may be predicted [24]. In the recycled HDDR powders, the Nd-rich phase was available at the particle boundaries of EOL magnets after the completion of d-HDDR reaction which then experienced the redistribution via liquidus state transformation during the SPS reprocessing at T ≥ 700 °C. Therefore, the H_{Ci} of SPS-ed magnets is higher than the starting recycled HDDR powder. It is evident that SPS allows controlled high heating rates which are suitable for rapid sintering of dense materials. The pulsed current and resistance heating at interparticle interfaces create very high localized temperature profiles, such that extensive mass transport is enhanced by grain boundary diffusion and pore annihilation [48,50]. Subsequently, faster cooling rates prevent the long-range diffusional transformation and grain growth can be controlled.

3.4. Magnetic properties and characterization of SPS-ed and thermally treated recycled HDDR powder

The effect of thermal treatment annealing was further studied on the recycled HDDR powder treated with SPS. The 750 °C temperature for 15 min holding time was chosen to compare the findings with the previous findings of K. Takagi et al. [23]. Thermal treatment temperature ternary eutectic point of 665 °C is set such that equilibrium diffusional mass transport can take place [51], and the Nd-rich phase can penetrate more intergranular channels so that the grain boundary phase distribution becomes more uniform. This temperature has experimentally proven to prevent the grain

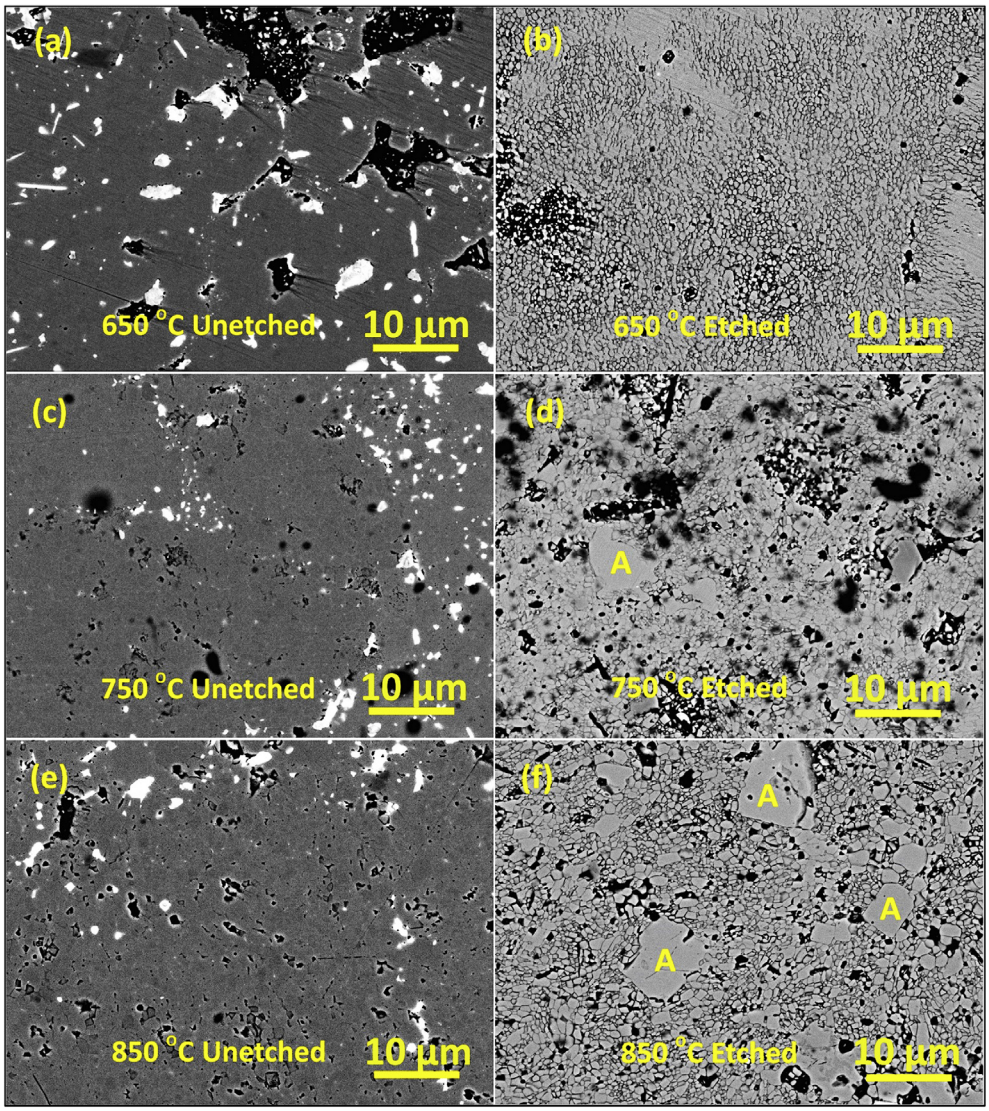

Fig. 5. BSE SEM micrographs of SPS-ed specimen: unetched surface at (a) 650 °C (c) 750 °C and (e) 850 °C; and etched surfaces showing grain structure at (b) 650 °C (d) 750 °C and (f) 850 °C. The increment of SPS temperatures from 650 to 850 °C indicates the evident grain coarsening at higher reprocessing temperatures; "A" features abnormal grain coarsening in samples SPS-ed at elevated temperatures.

coarsening, which will certainly reduce the H_{Ci}. This post SPS annealing temperature cannot be reciprocated within the SPS furnace due to a different localized heating mechanism [48–50]. In SPS, the excessive localized heating at interparticle contacts will contribute to the coarsening of the Nd-rich pools as well as the nanocrystalline grains. Since the Nd-rich phase will not be uniformly distributed as required for improving the H_{Ci}, further prolonging the holding time at 750 °C in the SPS has degraded the magnetic properties as shown in Table 2 (see below). Under conventional annealing treatments, the equilibrium diffusional heating [51] is applicable and the Nd-rich phase is allowed to redistribute via concentration gradients along the matrix grain surfaces [45–47].

The trend in Fig. 6 shows a comparative increase in H_{Ci} of thermally treated samples over that of the as SPS-ed samples (Fig. 4), but the H_{Ci} increase is milder in samples SPS-ed at temperatures higher than 750 °C. The sample SPS-ed at 650 °C experienced a substantial improvement in the $H_{Ci} = 1160$ kA/m from 790 kA/m. This is approximately 30% higher than the starting HDDR powder. The H_{Ci} increased only slightly for thermally treated samples SPS-ed at 850 °C due to the breach of grain growth temperature above 820 °C [23]. The B_r, BH_{max} and density of the thermally treated samples also experienced a mild improvement in absolute values in all cases as shown in Fig. 6. After the thermal treatment $B_r = 0.78$ T and $BH_{max} = 105$ kJ/m^3 was measured for the sample SPS-ed at 800 °C; however, the J_r/J_S ratio of 0.54 reaffirmed the 'isotropic nature' of reprocessed magnets. In the sample SPS-ed 850 °C a notable reduction in H_{Ci} negates the application of higher SPS temperatures for the recycled HDDR powder since this temperature is above the grain growth temperature [23].

The post-SPS equilibrium diffusion controlled thermal treatment is done to uniformly redistribute this liquid Nd-rich phase, smoothen the matrix and grain boundary interface, by reducing the interfacial strains associated with hcp Nd_2O_3 formation [23,25,35,40]. Therefore these treatments have also been reported to increase the H_{Ci} by the redistribution of Nd-rich grain boundary phase surrounding $Nd_2Fe_{14}B$ grains in sintered magnets [40–42] due to the localized decoupling of $Nd_2Fe_{14}B$ grains. Similarly, in the HDDR Nd-Fe-B magnets, the effect of localized decoupling can be combined with the domain wall pinning effect of the grain

Table 2
The variation of magnetic properties by altering SPS conditions and the improvement with annealing.

Table 2: The variation of magnetic properties by altering SPS conditions and the improvement with annealing.									
SPS Conditions ↓	100 ^{O}C/min Ramp and **1** minute holding time.			50 ^{O}C/min Ramp and **1** minute holding time.			100 ^{O}C/min Ramp and **5** minute holding time.		
SPS Temperature (^{O}C)	H_{Ci} (kA/m)	B_r (T)	Density (g/cm^3)	H_{Ci} (kA/m)	B_r (T)	Density (g/cm^3)	H_{Ci} (kA/m)	B_r (T)	Density (g/cm^3)
650	790 ↓ 1160	0.71 ↓ 0.75	6.96 ↓ 7.31	741 ↓ 1130	0.69 ↓ 0.72	7.01 ↓ 7.08	781 ↓ 1140	0.68 ↓ 0.70	7.13 ↓ 7.42
700	946 ↓ 1135	0.76 ↓ 0.76	7.49 ↓ 7.54	893 ↓ 1108	0.74 ↓ 0.75	7.36 ↓ 7.39	888 ↓ 1107	0.74 ↓ 0.75	7.51 ↓ 7.56
750	1061 ↓ 1120	0.76 ↓ 0.77	7.54 ↓ 7.56	1019 ↓ 1100	0.76 ↓ 0.77	7.53 ↓ 7.55	1040 ↓ 1102	0.75 ↓ 0.75	7.56 ↓ 7.57
800	1030 ↓ 1090	0.77 ↓ 0.78	7.55 ↓ 7.57	980 ↓ 1074	0.76 ↓ 0.77	7.55 ↓ 7.56	992 ↓ 1064	0.75 ↓ 0.75	7.57 ↓ 7.58
850	940 ↓ 1030	0.76 ↓ 0.77	7.56 ↓ 7.57	700 ↓ 790	0.68 ↓ 0.69	7.53 ↓ 7.56	855 ↓ 953	0.72 ↓ 0.74	7.57 ↓ 7.58

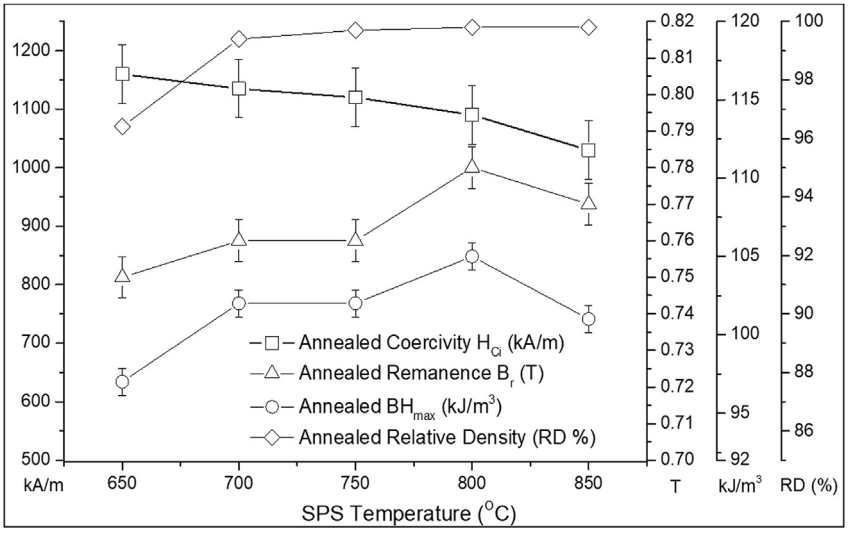

Fig. 6. The effect of post-SPS thermal treatment at 750 °C for 15 min on the H_{Ci}, B_r, BH_{max} and densification of the reprocessed HDDR Nd-Fe-B powders.

boundaries [23,35]. For the HDDR powders, the post-sinter annealing mechanism for the H_{Ci} improvement to date is not fully understood. According to K. Takagi et al. [23] the relaxation of interfacial strains is believed to improve the H_{Ci} in SPS-ed HDDR type magnets and suggested annealing did not change the thickness of the grain boundary phase. Whereby Li et al. [40], proposed

the increase in H_{Ci} after annealing is due to the widening of the amorphous Nd-rich grain boundary phase. According to W. Mo et al. [46], the grain boundary phase transforms from crystalline to amorphous as its thicknesses decrease, and in the case of HDDR Nd-Fe-B the grain boundary thickness varies from 1.6 to 3.0 nm only [23,33–35]. The thermal treatment temperature of 750 °C is adequately higher than the ternary eutectic (T_{ELM}) = 665 °C, so according to the pseudobinary phase diagram [39], the $Nd_2Fe_{14}B$ matrix and $NdFe_4B_4$ phases are in solid state but only the Nd-rich phase melts and undergoes diffusion controlled redistribution and therefore the thermal treatment should not contribute to grain growth significantly. The Nd oxide phases (hcp Nd_2O_3 and fcc NdO_X) also remain in the solid state during SPS-ing and thermal treatment but can experience the relaxation of the localized strain fields. Since T_{ELM} gets reduced due to the presence of Dy and Al from 685 °C to 665 °C [39], the Nd-rich phase must have high mobility at 750 °C for grain boundary diffusion, developing a controlled Nd-rich/$Nd_2Fe_{14}B$ interfacial microstructure for higher H_{Ci}. Therefore, one may speculate the redistribution of Nd-rich phase and relaxation of interfacial strains (at $Nd_2Fe_{14}B$ matrix grains, Nd-rich grain boundary phase and Nd oxide interjunctions) as a combined mechanism behind the H_{Ci} improvement in the SPS-ed and post-annealed HDDR system. When the SPS temperature is higher than T_{ELM}, then the short-range redistribution of the grain boundary phase can be attributed to the increased H_{Ci}. The complex microstructural effects associated with the Nd-rich phase and the interfacial grain chemistry as the governing mechanism behind the H_{Ci} enhancement in the HDDR powder is not properly understood. The H_{Ci} increase in the HDDR powder is associated with increased grain boundary width for effective grain decoupling from the ferromagnetic intergranular phase [33–35] as well as strain relaxation effects after the thermal treatment [23].

The most prominent feature from the microstructural comparison of SPS-ed unetched samples in Fig. 5 (a, c and e) with the post SPS thermally treated samples in Fig. 7 (a, c and e) attributed to the redistribution of the Nd-rich phase such that the areal fraction of thermally treated samples is higher than SPS reprocessed samples. On the contrary, when thermally treated specimens were etched, the difference in average grain size was minimal after the thermal treatment as evident in Fig. 7 (b, d and f) for 650, 750 and 850 °C respectively for the SPS reprocessed samples. Apart from normally grown nanocrystalline grains, the residual grains "R" from the EOL scrap magnets were also observed in the etched samples as shown in Fig. 7 (b and d). When the SPS reprocessing temperature was 650 °C, these residual grains were present without any expected increase in size because of the unavailability of the liquid phase to allow diffusion and grain growth [51]. The residual grains start faceting at T > 750 °C such that these large sized residual grains with more than 6 facets allow size augmentation due to excess thermal energy available at elevated SPS temperatures and so the normal grain growth is commenced [33]. At SPS temperature set at 850 °C, the residual, as well as larger nanocrystalline matrix grains, start consuming smaller grains and now the mechanism of grain growth proceeds to abnormal grain coarsening as shown in Fig. 7 (f). The abnormally coarsened grains contain isolated porosity, which makes them easier to distinguish from the residual grains. When the grain growth rate is higher than the pore mobility and the pores have surface energy higher than the grain boundary energy, then these pores get isolated within the abnormally coarsened grains and do not annihilate [51]. This, in turn, degrades the H_{Ci} at complete densification, as shown for thermally treated samples in Fig. 6.

From Fig. 8 (a) it can be observed that the 2:14:1 matrix grains are surrounded by the Nd-rich phase in the region approximately 1–2 μm away from the spot where Nd-rich phase has solidified after the SPS. The $Nd_2Fe_{14}B$ grains, further away approx. 10–20 μm from this region with the solidified Nd-rich phase, are observed to be in intimate contact with each other, as the grain boundary Nd-rich phase is absent or inadequately redistributed due to most probably short sintering times (10 min in total) and low temperatures (<750 °C) used in SPS.

After the thermal treatment performed in vacuum at 750 °C for 15 min, where the diffusion of the liquid phase is favorable (as the temperature exceeds the melting point of the Nd-rich phase), therefore the Nd-rich phase better surrounds the $Nd_2Fe_{14}B$ grains than in the SPS-ed samples from the condensed liquid phase. In the post thermally treated sample presented in Fig. 8 (b) it can be observed that instead of the Nd-pool a cavity appears in its place indicating to the Nd-rich phase has redistributed along the grain boundary channels to higher extent and longer lengths than in the SPS-ed only sample, as in Fig. 8 (a). This, in turn, results in an improvement in H_{Ci}, which was only slight for temperatures above 750 °C. This indicates that the SPS reprocessing parameters, especially the current density and temperature, have a more significant effect in developing the final microstructure and the magnetic properties. The thermal treatments are considered as a complementary process to further augment the magnetic properties by relieving the microstructure of the stresses and redistribution of RE-rich grain boundary phase [23,25,35,40].

The study also examined how the magnetic properties of the reprocessed HDDR powder are influenced by the alteration of two SPS processing conditions: the holding time (1 and/or 5 min) and the SPS heating rate (50 and/or 100 °C/min), as shown in Table 2. The arrows (↓) in Table 2 indicate the improvement in the magnetic properties of SPS-ed magnets after the thermal treatment at 750 °C for 15 min. This helped in determining the optimal reprocessing conditions at 50 MPa applied uniaxial pressure. The observed trend of best achieved magnetic properties (green table), as shown in Figs. 4 and 6, was by keeping the heating rate of 100 °C/minute and short holding time of 1 min only. Slowing the thermal ramp to 50 °C/minute did not add any improvement to the former case, so a rapid reprocessing approach is not detrimental as long as current density in the SPS is kept optimal [48,50]. Slower ramps slacken the short-range diffusivity and the redistribution of the Nd-rich liquid phase diminishes due to a lower SPS current density. At SPS temperature of 750 °C, the drop in H_{Ci} is insignificant even by prolonging the holding time due to better diffusion kinetics of the Nd-rich liquid phase. The magnetic properties degraded severely when the SPS temperature was higher than 820 °C, which is associated with the abnormal grain growth [23,37] and the results (from Figs. 5 and 7 of samples SPS-ed at 850 °C) are in agreement with these findings. Therefore, reducing the ramp at higher temperatures permits excess thermal energy to the system for grain coarsening. In the last case, when the holding temperature was increased to 5 min and the ramp was optimized to 100 °C/minute, the only persistent improvement observed was in the densification of the SPS-ed and thermally treated samples. The H_{Ci} was consistently higher than slower ramped samples (50 °C/min), but nonetheless, H_{Ci} was slightly lower than for the shorter holding time of 1 min. Although it can be expected that with higher overall densification, B_r, in turn, should increase, but the maximum value 0.75 T achieved disapproves the prolonged SPS holding times. Moreover, the abnormal grain growth kinetics can be activated with longer holding time and higher temperatures [48]. So by purpose, the SPS process has been verified as a significantly advantageous tool if the appropriate parameters are set for rapid sintering operations.

It is imperative to mention that SPS reprocessing is one of the few suitable techniques to obtain fully dense and high coercivity sintered magnets from the recycled HDDR powder since

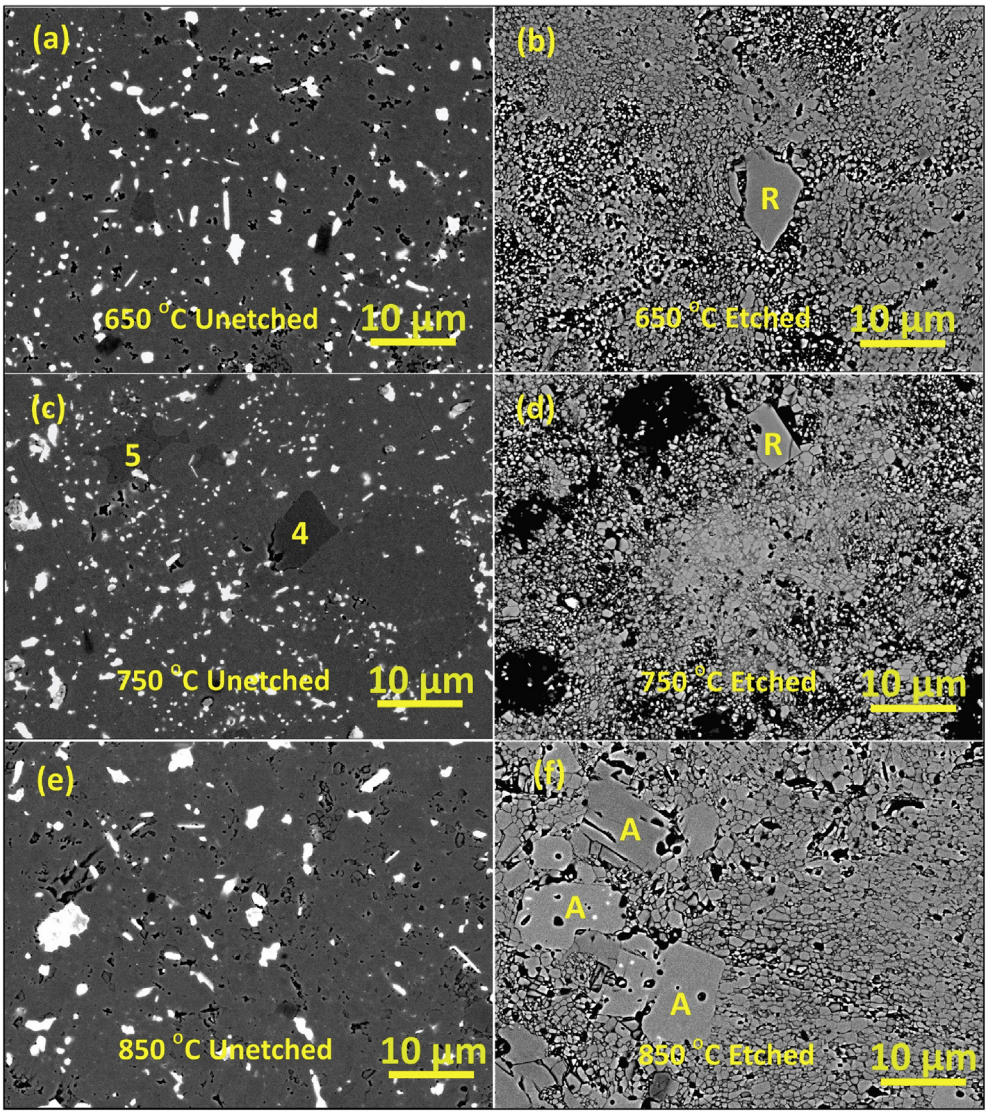

Fig. 7. BSE SEM micrographs of post SPS thermally treated: non-etched samples with better redistribution of Nd-rich grain boundary phase at (a) 650 °C (c) 750 °C and (e) 850 °C; and grain morphology of etched SPS-ed specimen at (b) 650 °C (d) 750 °C and (f) 850 °C; the grain marked with "R" indicate untransformed residual grains from EOL scrap magnet, "A" abnormally grown grains, "L" is $NbFe_2$ Type-Laves phase and "B" indicates tetragonal $NdFe_4B_4$ phase.

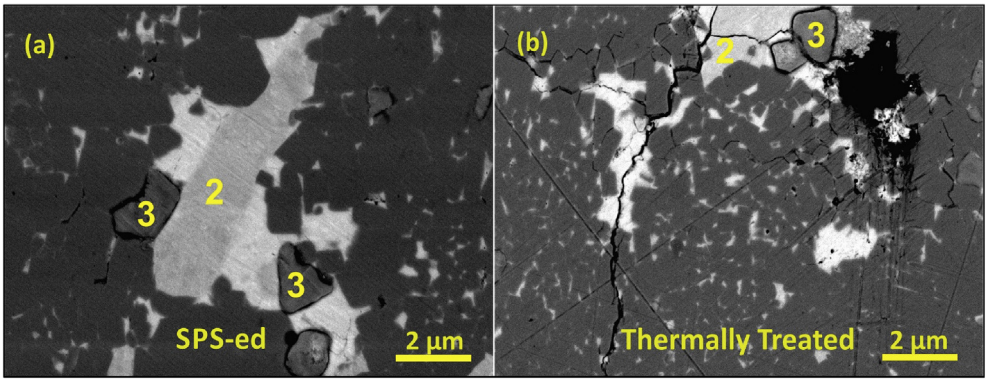

Fig. 8. High magnification micrographs showing the effect of grain boundary phase redistribution in (a) as SPS-ed sample synthesized at 750 °C and (b) thermally treated after SPS Phase 2 and 3 corresponds to Nd-rich phase and Nd_2O_3 respectively.

conventional vacuum sintering was not applicable to the recycled scrap and to our experience have produced poor results. This lack of sinterability in conventional vacuum sintering of the recycled HDDR powder is associated with the poor grain boundary phase

mobility and redistribution even at 1050 °C, therefore the powder particles do not coalescence together even in a well prepared green compact up to 100 MPa pressure. The simultaneous application of pressure and localized heating of powder particles in SPS allows the sintering to develop bulk magnet from scrap magnetic powders.

To summarize, the recycled HDDR Nd-Fe-B powder was subjected to a thorough SPS treatment. In all conditions, the coercivities of sintered magnets were higher than the starting recycled HDDR powder of average size 240 ± 100 nm due to the grain size preservation after the SPS reprocessing. The optimal temperature range of 750–800 °C for developing SPS-ed magnets was identified for reaching nearly full density and H_{Ci} higher than the starting recycled HDDR powder. Post SPS thermal treatment at 750 °C for 15 min increased the H_{Ci} due to the redistribution of thin Nd-rich grain boundary phase between the matrix grains, as confirmed by HR-SEM. The effect of redistribution is pronounced after thermal treatment above eutectic temperature on the samples SPS-ed at 650 °C due to limited diffusion in the solid state SPS. Whereby above the eutectic point, the sample SPS-ed at 700 °C experienced a higher degree of wetting of the matrix grains and subsequently the H_{Ci} was high after SPS. The SPS-ed samples reached peak H_{Ci} of 1060 kA/m value after SPS at 750 °C, whereby the full densification was achieved by SPS at 800 °C which can be associated with effective pore elimination. The post-SPS thermal treatment resulted in the H_{Ci} improvement up to 30% higher than the starting recycled HDDR powder. The samples SPS-ed at lower temperatures like 650–750 °C experienced improvement in the H_{Ci} due to better redistribution of Nd-enrichments from the particle to the grain boundaries. No evidence of abnormal grain growth was observed after the subsequent reprocessing with SPS and thermal treatment under the optimum conditions. The average grain size of samples SPS-ed at 650 °C and 750 °C were 280 ± 120 nm, and 330 ± 120 nm respectively. Post thermal treatments did not exaggerate the grain size and the average grain size only experienced a modest increment of approx. 100–200 nm. The magnetic properties begin to deteriorate when SPS temperature was greater than 800 °C due to a breach of grain growth temperature and defect generation due to localized overheating during the SPS. While the samples SPS-ed at T ≥ 850 °C, a modest gain in the H_{Ci} was reported after the thermal treatment, which may be associated only with the relaxation of the interfacial strains introduced by defects generation along the coarser grains. For the samples SPS-ed at 850 °C the normal grains ranged from 400 ± 250 nm whereby coarser grains extended from 750 to 2600 nm making a bimodal size distribution. Slowing down the SPS heating rate to 50 °C/minute did not add to the improvement of the H_{Ci}. Also, increasing the holding time to 5 min only improved the densification, but not the H_{Ci}. Disclosing the mechanism behind H_{Ci} enhancement in terms of the microstructure after SPS reprocessing and the post-sinter thermal treatment signifies the magnetic performance relationship to develop suitable reuse and recyclability of the EOL/scrap magnets as well as the applicability of SPS reprocessed permanent magnets.

4. Conclusions

The two accomplished goals of this study include: reprocessing of the recycled HDDR Nd-Fe-B powders with SPS and thermal treatment in combination delivered fully dense bulk magnets with H_{Ci} values synonymous to the SPS-ed commercial grade Aichi Steel's HDDR powder. Secondly, even with a high oxygen content in the recycled powders (~4760 ppm), sinterability was not lost and the SPS-ed H_{Ci} was higher than the starting HDDR. This route also verified 100% preservation of H_{Ci} of the EOL scrap magnets by HDDR nano structurization and subsequent SPS treatment. The SPS performed below the eutectic do not provide enough grain boundary phase in the liquid state, so after the thermal treatment at 750 °C, which is above the eutectic temperature, the melt formation wets the grain boundaries and H_{Ci} is increased due to a better redistribution of the liquid phase from particle junctions it diffuses more along the nanocrystalline grains. Whereas the SPS reprocessing at 750 °C already has the intergranular Nd-rich phase in a liquid state and it begins to further wet as the liquid phase is redistributed under continuous uniaxial pressure from SPS. This short-order redistribution of the Nd-rich grain boundary phase at optimal SPS conditions is the proposed reason for the H_{Ci} higher than the starting recycled HDDR powder. Only a slight grain growth of <100 nm on average from the recycled HDDR powder was identified after SPS-ing in the optimal conditions. The Nd-rich phase redistribution is effective for samples SPS-ed below the abnormal grain growth temperature of 820 °C as the liquid phase has already wetted the nanocrystalline grain boundary channels and the particle boundaries. At 850 °C the nanocrystalline grains grew to the size range of 750–2600 nm and in parallel, the residual grains also experience grain coarsening and grow to size larger than ≥10 μm, with both processes the normal and the abnormal grain growth °Ccurring simultaneously. Due to the abnormal grain growth kinetics at elevated temperature, the pores were observed to be isolated within the coarsened grains. These pores in larger grains create internal tension and as the grains expand in size, the microstructure might experience a localized strain from the grain boundaries and secondary phases. At this point (>820 °C), the localized SPS overheating (high current density and Joule's heating effect) causes the larger grains to grow at the expense of smaller nanocrystalline grains and Nd-enrichments which might generate a number of defects along the coarser grains, so the post-SPS thermal treatment may also contribute in the relaxation of the interfacial strains which increases the H_{Ci} (approx. 5–10%) and not just to the Nd-rich phase redistribution especially for the samples SPS-ed above 820 °C. Thereby the strain in the microstructure at elevated SPS conditions can be associated with the high current density due to Joules heating, pore segregation, Ostwald ripening and secondary phases compressing the matrix grains. After the thermal treatment, the microstructure is relaxed of the strain arising from the SPS reprocessing. The observed grain growth after the thermal treatment is less than 100–150 nm in optimally SPS reprocessed sample at 750 °C. Upon that the SPS and thermal treatment in combination are the ideal tools to preserve the coercivity of the initial HDDR powder and therefore ideal to reprocess the recycled magnet scrap to sintered magnets. The SPS temperatures >820 °C should be avoided as it activates the Ostwald ripening and degrades the magnetic properties.

Acknowledgments

The research leading to these results has received the funding from the European Community's Horizon 2020 Program ([H2020/2014-2019]) under Grant Agreement no. 674973 (MSCA-ETN DEMETER), Belgium. Project website: http://etn-demeter.eu/. This publication reflects only the authors' views, which are targeted to contribute to the betterment of the global community. The authors would also like to acknowledge the Department for Nanostructured Materials (K7 Nano) for the provision of the reprocessing facilities and Center for Electron Microscopy & Microanalysis (CEMM) for analytical scanning electron microscopy at the Jozef Stefan Institute Slovenia. We also extend our thanks on the support offered Mr. Luka Kelhar (MSc.) for the XRD analysis at JSI Slovenia.

References

[1] M. Sagawa, S. Fujimura, N. Togawa, Y. Matsuura, New material for permanent

magnet on a base of Nd and Fe, J. Appl. Phys. 55 (1984) 2083.
[2] J.J. Croat, J.F. Herbst, R.W. Lee, F.E. Pinkerton, Pr-Fe and Nd-Fe-based materials: a new class of high performance permanent magnets, J. Appl. Phys. 55 (1984) 2078.
[3] H.R. Kirchmayr, Permanent magnets and hard magnetic materials, J. Phys. D Appl. Phys. 29 (1996) 2763–2778.
[4] S. Sugimoto, Current status and recent topics of rare-earth permanent magnets, J. Phys. D Appl. Phys. 44 (2011), 064001.
[5] Poudyal Narayan, J Ping Liu, Advances in nanostructured permanent magnets research, J. Phys. D Appl. Phys. 46 (2013), 043001 pg. 23.
[6] Critical Raw Materials for the EU, European Commission, Brussels, Belgium, 2014.
[7] Xiantao Li, Ming Yue, Zakotnik Miha, Weiqiang Liu, Dongtao Zhang, Tieyong Zuo, Regeneration of waste sintered Nd-Fe-B magnets to fabricate anisotropic bonded magnets, J. Rare Earths 33 (No. 7) (2015) 736.
[8] O. Gutfleisch, M.A. Willard, E. Brück, C.H. Chen, S.G. Sankar, J.P. Liu, Magnetic materials and devices for the 21st century: stronger, lighter, and more energy efficient, Adv. Mater. 23 (2011) 821.
[9] A. Walton, Yi Han, N.A. Rowson, J.D. Speight, V.S.J. Mann, R.S. Sheridan, A. Bradshaw, I.R. Harris, A.J. Williams, The use of hydrogen to separate and recycle neodymium iron boron-type magnets from electronic waste, J. Clean. Prod. 104 (2015) 236–241.
[10] C. Li, W.Q. Liu, M. Yue, Y.Q. Liu, D.T. Zhang, T.Y. Zuo, Waste Nd-Fe-B sintered magnet recycling by doping with rare earth rich alloys, IEEE Trans. Magn. 50 (2014), 2105403.
[11] B. Sprecher, Y.P. Xiao, A. Walton, J. Speight, R. Harris, R. Kleijn, G. Visser, G.J. Kramer, Life cycle inventory of the production of rare earths and the subsequent production of NdFeB rare earth permanent magnets, Environ. Sci. Technol. 48 (2014) 3951.
[12] E.A. Périgo, S.C. da Silva, R.V. Martin, H. Taklishi, F.J.G. Landgraf, Properties of hydrogenation-disproportionation-desorption-recombination NdFeB powders prepared from recycled sintered magnets, J. Appl. Phys. 111 (2012), 07A725.
[13] R.S. Sheridan, R. Sillitoe, M. Zakotnik, I.R. Harris, A.J. Williams, Anisotropic powder from sintered NdFeB magnets by the HDDR processing route, J. Magn. Magn. Mater. 324 (2012) 63.
[14] M. Zakotnik, I.R. Harris, A.J. Williams, Possible methods of recycling Nd-Fe-B-type sintered magnets using the HD/degassing process, J. Alloys Compd. 450 (2008) 525.
[15] M. Zakotnik, I.R. Harris, A.J. Williams, Multiple recycling of NdFeB-type sintered magnets, J. Alloys Compd. 469 (2009) 314.
[16] M. Itoh, M. Masuda, S. Suzuki, K. Machida, Recycling of rare earth sintered magnets as isotropic bonded magnets by melt-spinning, J. Alloys Compd. 374 (2004) 393.
[17] O. Gutfleisch, K. Güth, T.G. Woodcock, Recycling used Nd-Fe-B sintered magnets via a hydrogen-based route to produce anisotropic, resin bonded magnets, Adv. Energy Mater. 3 (2013) 151.
[18] M. Itoh, M. Masuda, S. Suzuki, K. Machida, Recycle for sludge scrap of Nd-Fe-B sintered magnet as isotropic bonded magnet, J. Rare Earths 22 (2004) 168.
[19] A.S. Kim, D.H. Kim, S. Namkung, T.S. Jang, D.H. Lee, H.W. Kwon, D.H. Hwang, Development of high coercive powder from the Nd-Fe-B sintered magnet scrap, IEEE Trans. Magn. 40 (2004) 2877.
[20] P.J. McGuiness, C. Short, A.F. Wilson, I.R. Harris, J. Alloys Compd. 184 (1992) 243–255.
[21] K.H. Müller, W. Grünberger, D. Hinz, B. Gebel, D. Eckert, A. Handstein, Mater. Lett. 34 (1998) 50–54.
[22] K. Suresh, T. Ohkubo, Y.K. Takahashi, K. Ohishi, R. Gopalan, K. Hono, T. Nishiuchi, N. Nozawa, S. Hirosawa, Consolidation of hydrogenation–disproportionation–desorption– recombination processed Nd–Fe–B magnets by spark plasma sintering, J. Magn. Magn. Mater. 321 (2009) 3681–3686.
[23] K. Takagi, M. Akada, R. Soda, K. Ozaki, Preparation of Nd–Fe–B sintered magnets from HDDR-processed powder, J. Magn. Magn. Mater. 393 (2015) 461–466.
[24] R. Gopalan, H. Sepehri-Amin, K. Suresh, T. Ohkubo, K. Hono, T. Nishiuchi, N. Nozawac, S. Hirosawac, Anisotropic Nd–Fe–B nanocrystalline magnets processed by spark plasma sintering and in situ hot pressing of hydrogenation–decomposition–desorption–recombination powder, Scr. Mater. 61 (2009) 978–981.
[25] W.F. Li, T. Ohkubo, K. Hono, T. Nishiuchi, S. Hirosawa, Coercivity mechanism of hydrogenation disproportionation desorption recombination processed Nd–Fe–B based magnets, Appl. Phys. Lett. 93 (2008), 052505.
[26] N. Nozawa, H. Sepehri-Amin, T. Ohkubo, K. Hono, T. Nishiuchi, S. Hirosawa, J. Magn. Magn. Mater. 323 (2011) 115–121.
[27] H. Nakamura, K. Hirota, M. Shimao, T. Minowa, M. Honshima, Magnetic properties of extremely small Nd–Fe–B sintered magnets, IEEE Trans. Magn. 41 (No. 10) (2005).
[28] H.W. Kwon, J.G. Lee, J.H. Yu, Origin of radical coercivity reduction in fine Nd-Fe-B-type hydrogenation, disproportionation, desorption, recombination particles and its recovery, J. Appl. Phys. 115 (2014) 17A727.
[29] R.S. Sheridan, A.J. Williams, I.R. Harris, A. Walton, Improved HDDR processing route for production of anisotropic powder from sintered NdFeB type magnets, J. Magn. Magn. Mater. 350 (2014) 114–118.
[30] Z.H. Hu, M.G. Zhu, W. Li, F.Z. Lian, Effects of Nb on the coercivity and impact toughness of sintered Nd-Fe-B magnets, J. Magn. Magn. Mater. 320 (3–4) (2008) 96–99.
[31] F.M. Ahmed, I.R. Harris, Improvement of microstructure and magnetic properties of NdFeB alloys by Nb and Co additions, J. Magn. Magn. Mater. 320 (2008) 2808–2813.
[32] N. Oono, M. Sagawa, R. Kasada, H. Matsui, A. Kimura, Production of thick high-performance sintered neodymium magnets by grain boundary diffusion treatment with dysprosium–nickel–aluminum alloy, J. Magn. Magn. Mater. 323 (2011) 297–300.
[33] K. Morimoto, N. Katayama, H. Akamine, M. Itakura, Coercivity enhancement of anisotropic Dy-free Nd–Fe–B powders by conventional HDDR process, J. Magn. Magn. Mater. 324 (2012) 3723–3726.
[34] H. Sepehri-Amin, T. Ohkubo, T. Nishiuchi, S. Hirosawa, K. Hono, Coercivity enhancement of hydrogenation–disproportionation–desorption–recombination processed Nd–Fe–B powders by the diffusion of Nd–Cu eutectic alloys, Scr. Mater. 63 (2010) 1124–1127.
[35] W.F. Li, T. Ohkubo, K. Hono, T. Nishiuchi, S. Hirosawa, The role of grain boundaries in the coercivity of hydrogenation disproportionation desorption recombination processed Nd–Fe–B powders, J. Appl. Phys. 105 (2009), 07A706.
[37] Xiao-Qiang Li, Li Li, Ke Hu, Zhi-Cheng Chen, Sheng-Guan Qu, Chao Yang, Microstructure and magnetic properties of anisotropic Nd–Fe–B magnets prepared by spark plasma sintering and hot deformation, Trans. Nonferrous Met. Soc. China 24 (2014) 3142–3151.
[38] Randall M. German, Pavan Suri, Seong Jin Park, Review: liquid phase sintering, J. Mater. Sci. 44 (2009) 1D39.
[39] U.M.R. Seelam, T. Ohkubo, T. Abe, S. Hirosawa, K. Hono, Faceted shell structure in grain boundary diffusion-processed sintered Nd–Fe–B magnets, J. Alloys Compd. 617 (2014) 884–892.
[40] W.F. Li, T. Ohkubo, K. Hono, Effect of post-sinter annealing on the coercivity and microstructure of Nd–Fe–B permanent magnets, Acta Mater. 57 (2009) 1337–1346.
[41] W. Li, T. Ohkubo, T. Akiya, H. Kato, K. Hono, The role of Cu addition in the coercivity enhancement of sintered Nd-Fe-B permanent magnets, J. Mater. Res. 24 (2009) 413–420.
[42] F. Vial, F. Joly, E. Nevalainen, M. Sagawa, K. Hiraga, K.T. Park, Improvement of coercivity of sintered NdFeB permanent magnets by heat treatment, J. Magn. Magn. Mater. 242–245 (2002) 1329–1334.
[44] W.F. Li, T. Ohkubo, K. Hono, M. Sagawa, The origin of coercivity decrease in fine grained Nd-Fe-B sintered magnets, J. Magn. Magn. Mater. 321 (2009) 1100–1105.
[45] M. Matsuura, R. Goto, N. Tezuka, S. Sugimoto, Influence of Nd oxide phase on the coercivity of Nd-Fe-B thin films, Mater. Trans. 51 (10) (2010), 1901 to 1904.
[46] W. Mo, L. Zhang, Q. Liu, A. Shan, J. Wu, M. Komuro, Dependence of the crystal structure of the Nd-rich phase on oxygen content in an Nd–Fe–B sintered magnet, Scr. Mater. 59 (2008) 179–182.
[47] T. Fukagawa, S. Hirosawa, Influence of $Nd/Nd_2Fe_{14}B$ interface microstructure on the coercivity of surface $Nd/Nd_2Fe_{14}B$ grains in Nd-sputtered Nd–Fe–B sintered magnets, Scr. Mater. 59 (2008) 183–186.
[48] R. Orru, R. Licheri, A. Mario Locci, A. Cincotti, G. Cao, Consolidation/synthesis of materials by electric current activated/assisted sintering, Mater. Sci. Eng. R Rep. 63 (2009) 127–287.
[49] T. Hungrı, J. Galy, A. Castro, Spark plasma sintering as a useful technique to the nanostructuration of piezo-ferroelectric materials, Adv. Eng. Mater. 11 (2009) 8.
[50] Z. Zhang, Z. Liu, J. Lu, X. Shen, F. Wang, Y. Wang, The sintering mechanism in spark plasma sintering – proof of the occurrence of spark discharge, Scr. Mater. 81 (2014) 56–59.
[51] M.N. Rahaman, Ceramic Processing and Sintering, second ed., Marcel Dekker Inc, NY, USA, 2003.
[52] R.S. Sheridan, I.R. Harris, A. Walton, The development of microstructure during hydrogenation–disproportionation–desorption–recombination treatment of sintered neodymium-iron-boron-type magnets, J. Magn. Magn. Mater. 401 (2016) 455–462.

Further reading

[36] E. Galego, H. Takiishi, R. Nunes de Faria Jr., Magnetic properties of Pr-Fe-Co-B bonded HDDR magnets with alloying additions, Mater. Res. 10 (No. 3) (2007) 273–277.
[43] T.T. Sasaki, T. Ohkubo, K. Hono, Y. Une, M. Sagawa, Correlative multi-scale characterization of a fine grained Nd–Fe–B sintered magnet, Ultramicroscopy 132 (2013) 222–226.